Modelling transport-limited discharge capacity of lithium-sulfur cells

Teng Zhang[a,*], Monica Marinescu[a], Sylwia Walus[b], Gregory J. Offer[a]

[a] *Department of Mechanical Engineering, Imperial College London, SW7 2AZ, UK*
[b] *OXIS Energies Ltd, E1 Culham Science Centre, Abingdon, OX14 3DB, UK*

Abstract

Lithium-sulfur (Li-S) battery could bring a step-change in battery technology with a potential specific energy density of 500 - 600 Wh/kg. A key challenge for further improving the specific energy-density of Li-S cells is to understand the mechanisms behind reduced sulfur utilisation at low electrolyte loadings and high discharge currents. While several Li-S models have been developed to explore the discharge mechanisms of Li-S cells, they so far fail to capture the discharge profiles at high currents. In this study, we propose that the slow ionic transport in concentrated electrolyte is limiting the rate capability of Li-S cells. This transport-limitation mechanism is demonstrated through a one-dimensional Li-S model which qualitatively captures the discharge capacities of a sulfolane-based Li-S cell at different currents. Furthermore, our model predicts that a discharged Li-S cell is able regain some capacity with a short period of relaxation. This capacity recovery phenomenon is validated experimentally for different discharge currents and relaxation durations. The transport-limited discharge behavior of Li-S cells highlights the importance of optimizing the electrolyte loading and electrolyte transport property in Li-S cells.

Keywords: lithium-sulfur, discharge capacity, ionic transport, mathematical model

1. Introduction

Lithium sulfur (Li-S) battery is emerging as a prime candidate for post lithium-ion battery technologies due to its high practical specific energy density of 500 - 600 Wh/kg [1, 2]. Despite their presently limited cycle life, the superior specific energy density of Li-S cells already allows for niche applications, such as in the high-altitude unmanned air vehicle, Zephyr [3]. A key challenge in further enhancing the energy density of Li-S batteries is to identify the mechanisms behind the limited sulfur utilization, especially at higher discharge rates. To this end, a majority of Li-S literature have been focused on improving the sulfur utilization through materials research, whereas relevant studies from a mathematical modeling perspective have been rare.

*Corresponding author
Email address: t.zhang@imperial.ac.uk (Teng Zhang)

The discharge of a Li-S cell produces various intermediate polysulfide species that are soluble in typical aprotic solvents. It is generally believed that the dissolution of these polysulfide species into the electrolyte, and their subsequent diffusion away from electrochemically active surfaces, contribute to a major degradation mechanism as well as sulfur-utilization limitation [4, 5]. In light of this loss mechanism, numerous strategies have been proposed to encapsulate polysulfides in the cathode, including optimization of the cathode nanomorphology (as reviewed in [6, 7]), doping of polysulfide-adsorption sites [8, 9], and coating of polysulfide blocking or adsorption layers [10, 11]. However, most of these experimental studies are carried out with vast excess of electrolyte [12], not taking into account the fact that the electrolyte-to-sulfur mass ratio has a major influence on the sulfur utilisation [13, 14, 15]. In order to achieve high energy-density at cell level, the mass ratio between electrolyte and sulfur should be limited to below 3 [12]. In such cases, the electrolyte is highly concentrated, and the solubility and transport of the various species could be limiting the sulfur utilisation.

While several physics-based models have been developed for Li-S cells [16, 17, 18, 19, 20, 21, 22, 23, 24, 25, 26], they fail to capture the utilization of sulfur at different discharge currents, e.g. the rate capability. Kumaresan et al [17] developed the first 1D Li-S model that describes electrochemical reactions, precipitation and dissolution reactions, and ionic transport during discharge based on the Nernst-Plank equations. The model is able to qualitatively capture the discharge behavior of a Li-S cell at low currents. Sensitivity analysis of the Kumaresan model by Ghaznavi and Chen [20, 21, 22] indicates that at high discharge currents, the model predicts a capacity reduction in the high-plateau region while the change in low-plateau capacity is negligible. However, experimental Li-S cell discharge curves exhibit an opposite trend whereby increasing the discharge current reduces the cell's low-plateau capacity significantly but not its high-plateau capacity [27, 28]. The same mismatch between the experimental and modelled discharge behavior is also present in other similar Li-S models [18, 19].

In analysing the sensitivity of the Kumaresan model with respect to the diffusion coefficients of ions, Ghaznavi and Chen [22] noticed that the modelled low-plateau capacity would decrease when the effective ionic diffusion coefficients were reduced. With an effective lithium ion diffusion coefficient on the order of 10^{-12} m^2s^{-1}, the dissolving Li^+ ions build up a large concentration gradient in the separator which requires high concentrations of polysulfide anions in the separator to maintain charge neutrality. Based on the Kumaresan model [17], the high concentration of polysulfides in the separator would lead to the precipitation of Li_2S_2, Li_2S_4, and Li_2S_8. These precipitates would eventually block the separator/anode interface and cause a reduced discharge capacity. However, there has been no direct experimental evidence for the existence of any solid discharge product other than Li_2S in Li-S cells [29]. The modelled discharge profiles with low ionic diffusion coefficients were also not compared to experiments.

Recently, Danner et al [26] introduced a particle-scale model for Li-S cells in which polysulfides are confined only within nanostructured sulfur/carbon (S/C) particles. The model predicts the existence of a transport overpotential caused by the transport of Li^+ ions against a concentration gradient into the S/C particles. This Li^+ ion concentration gradient, arising from the high concentrations of polysulfide anions confined within the S/C

particles, leads to localized Li_2S precipitation during discharge which could cause pore-blocking and reduced sulfur utilisations at high sulfur loadings. This transport-limitation at the particle-scale is similar to the transport limitation scenario at the cell-scale predicted by the Kumaresan model with low ionic diffusion coefficients [22]. However, Danner et al noted that this transport-limitation effect was absent when modelling conventional cathodes where polysulfides were not confined.

This study presents a more detailed investigation into the discharge behavior of Li-S cells subjected to transport limitation. We show that with effective ionic diffusion coefficients on the order of 10^{-12} m^2s^{-1}, a modified Kumaresan model [17] is able to capture the rate capability of a 3.4 Ah Li-S pouch cell containing conventional composite cathodes. The reduction of low-plateau capacity at high discharge currents is explained by trapping of polysulfides in the separator as result of the slow transport of Li^+ ions through the separator. Based on this transport-limitation mechanism, the model predicts that a discharged Li-S cell is able to regain some capacity after a short period of relaxation. We validate this capacity recovery effect by comparing modelled and experimental recoverable capacities at different discharge currents and after various durations of relaxation.

2. Discharge modelling and experiments

2.1. The Li-S model

We employ the relatively well-studied Li-S model developed by Kumaresan et al [17] to investigate the discharge behaviour of Li-S cells. The model formulation, implementation, and parameters are summarized in Appendix A. Two major modifications to the Kumaresan model are made in order to capture the high-rate discharge behaviour of measured Li-S cells: First, we prohibit the precipitation of polysulfides (Li_2S_2, Li_2S_4, and Li_2S_8) other than Li_2S in the model, since Li_2S is the only experimentally detected solid discharge product in Li-S cells. Secondly, we reduce the effective ionic diffusion coefficients in the Kumaresan model by two orders of magnitudes to around 10^{-12} m^2s^{-1}, which was shown to cause transport limitation in the model [22]. The diffusion coefficients of dissolved polysulfides are not well-established in the literature due to the difficulties in isolating an individual polysulfide species that could rapidly disproportionate or associate. The diffusion coefficient of dissolved S_8 was estimated with rotating ring-disk electrode measurement to be on the order of 10^{-10} m^2s^{-1} in a dilute electrolyte containing mixtures of 1,2-dimethoxyethane and 1,3-dioxolane solvents [30]. The same quantity was estimated to be on the order of 10^{-12} to 10^{-11} m^2s^{-1} in a concentrated electrolyte containing a tetraglyme solvent based on steady-state cyclic voltammetry measurements using an ultramicroelectrode [27]. The Li-S cell under study contains sulfolane solvent which is known to exhibit an order of magnitude higher viscosity than most ether-based solvents [31], and is therefore likely to possess lower ionic diffusion coefficients as well.

The effective ionic diffusion coefficients in Li-S cells depend on the electrolyte composition, ionic concentrations, as well as the porosity and tortuosity of electrodes. In the present model, however, we take the simplifying assumption that ionic diffusion coefficients are independent of the electrolyte composition and ionic concentrations, so that the standard

Nernst-Planck equations for dilute solution can be applied to describe ionic transport in Li-S cells. We note that all existing Li-S models utilize dilute solution theory to describe ionic transport, even though it was found to be inaccurate in calculating the electrolyte resistance which is concentration-dependent [23]. This limitation is due to a lack of measured polysulfide transport properties, as well as the complexity of concentrated-solution theory (e.g. Maxwell-Stefan formulation) which would render the resulting Li-S model intractable. In addition, we employ the empirical Bruggeman relation (Eq. A22) frequently applied in both lithium-ion and Li-S battery models to describe the dependence of effective diffusion coefficients on the electrode morphology. However, we note that the Bruggeman relation with an exponent of 1.5 is derived for porous morphology made up of isotropic spheres [32], which is quite different from the carbon/sulfur composite morphology in which sulfur (or Li_2S) is dispersed in the pores of carbon matrix. Consequently, the model does not accurately capture the effect of carbon/sulfur morphology on ionic diffusivity. More complex approaches are required to adequately characterise the morphology-diffusivity relation, which may include image based modelling with 3D microstructure data obtained from tomography experiments [33].

2.2. Discharge measurements

A Li-S pouch cell (OXIS Energy Ltd) with a rated capacity of 3.4 Ah at 0.2 C was used to calibrate and validate the discharge curves generated by the model. The cell contains multiple layers of lithium foil anode, polymeric separator, and carbon/sulfur composite cathode filled with sulfolane solvent. Constant current discharges were performed at 30 ^{0}C with a Bio-Logic VMP3 potentiostat at 0.2C, 0.5C, and 1C discharge rates to a cut-off voltage of 1.5V. Two sets of capacity recovery experiments were conducted. In the variable discharge-rate tests, the cell was first discharged at a constant current of different magnitudes (0.2C, 0.5C, and 1C). The cell was then disconnected for 5 hours, before it was discharged again at 0.2C. In the variable rest-duration tests, the cell was discharged at 1C followed by a relaxation period of different lengths (10 minutes to 4 hours). It was then discharged again at 1C.

3. Results and discussion

The simulated discharge profiles at 0.2C, 0.5C and 1C rates are compared with the measured curves in Fig. 1. The model captures the reduction of low-plateau capacity at high discharge currents, which was not possible with previous Li-S models in the literature. Like previous 1D Li-S models, however, the present model is only able to qualitatively match with measurements, and larger deviations in cell voltage are seen at higher discharge currents. A major factor that contributes to this limitation is the inability of the existing Li-S models to capture the correct electrolyte-phase potential drop during discharge. Electrochemical impedance spectroscopy measurements have shown that the electrolyte resistance of a Li-S cell varies significantly during discharge, and the corresponding Ohmic potential drop represents the dominant voltage-loss mechanism in the high-plateau region [34, 35]. The present Li-S model based on Kumaresan et al, however, was shown to significantly underestimate

the electrolyte resistance due to the dilute-solution assumption [23]. Capturing the correct electrolyte resistance variation during discharge would require concentration-dependent ionic transport properties that are not established in the literature.

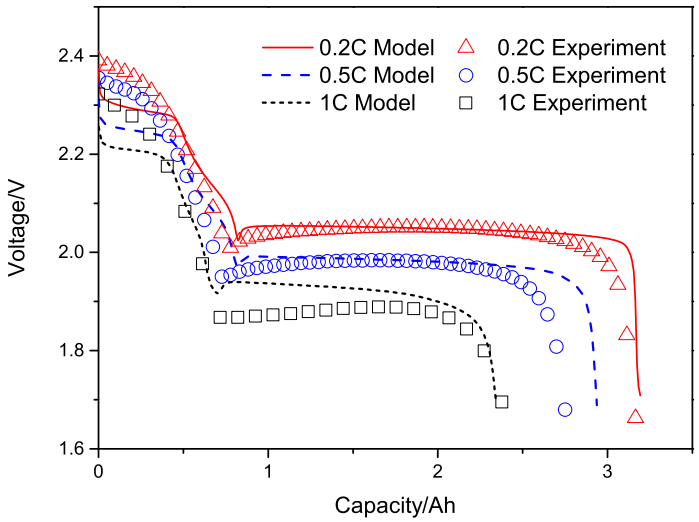

Figure 1: Measured (symbols) and simulated (lines) discharge curves at 0.2C, 0.5C, and 1C.

To understand the mechanisms behind the reduction of low-plateau capacity at high discharge currents, we examine the ionic concentration profiles across the cell at the end of discharge in Fig. 2. The slow Li^+ ion transport as a result of its low diffusion coefficient leads to the build-up of a large Li^+ ion concentration gradient across the separator. The Li^+ concentration gradient is much smaller in the cathode due to the rapid precipitation of Li_2S. Similar concentration gradients also exist for anion species such as S_4^{2-} and S_2^{2-}. While S_4^{2-} and S_2^{2-} anions are only produced electrochemically in the cathode, they subsequently migrate under the electric field into the separator in order to maintain charge neutrality. The high charge density of Li^+ ion near the anode effectively traps some polysulfide species in the separator. By the end of discharge, the amount of reducible S_4^{2-} and S_2^{2-} remaining in the separator represent a reduction in discharge capacity. Since the concentration gradients are larger at higher discharge currents, the reduction in discharge capacity is correspondingly greater.

In Ghaznavi and Chen's Li-S model with low ionic diffusion coefficients [22], the end of discharge is caused by pore-blocking near the anode as a result of Li_2S_2 and Li_2S_4 precipitation. Since the precipitated species do not re-dissolve significantly unless cell is charged, their model yields negligible capacity recovery during cell relaxation. The present model, in contrary, does not allow S_4^{2-} and S_2^{2-} anions to precipitate but instead lets them re-equilibrate across the cell during relaxation. Consequently, the model predicts the trapped S_4^{2-} and S_2^{2-} anions in the separator will gradually diffuse back into the cathode once dis-

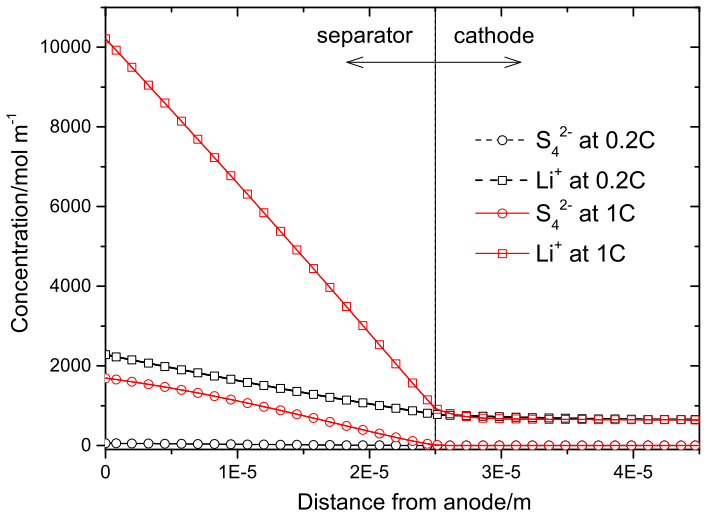

Figure 2: Simulated concentrations of Li^+ and S_4^{2-} ions across the cell at the end of 0.2C and 1C discharges.

charge is stopped, thereby allowing the cell to regain some capacity. The capacity recovery experiments were carried out to verify this model prediction.

Fig. 3 compares the experimental and modelled discharge capacities for both the first discharges at 0.2C, 0.5C, and 1C, and the second discharges at 0.2C performed after 5 hours of relaxation. While the model underestimates the recoverable capacities for the experiments with 0.2C and 0.5C first-discharge currents, it correctly predicts the trend of increasing second-discharge capacity with larger first-discharge current. The significant capacity recovery after 1C discharge strongly suggests that the discharge capacity reduction at high current is not solely caused by precipitation-induced pore-blocking or surface passivation, as both processes are unlikely to be reversible during cell relaxation. Furthermore, both measurements and simulations indicate the sum of the initial and the recovered discharge capacities are similar for all three discharge-relaxation-discharge scenarios. This match in total discharge capacity suggests the lost capacity during a high-rate discharge can be almost fully recovered through a 5-hour relaxation.

To further examine the time required to retrieve all of the recoverable capacity, we measured recoverable capacities after different durations of relaxation after discharge. It can be seen from Fig. 4 that the recoverable capacity reaches a plateau after just one hour of rest after a 1C discharge. Compared to measurements, the model-predicted capacity recovery rate is almost twice as fast: based on the model, a 30 minute rest is sufficient to retrieve most of the recoverable capacity. Fig. 5 demonstrates the modelled Li^+ ion concentrations at both ends of the separator throughout the discharge-relaxation-discharge process. The Li^+ ion concentration difference across the separator increases during discharge, and decreases during the relaxation as Li^+ ions diffuse into the cathode. Since the concentration difference

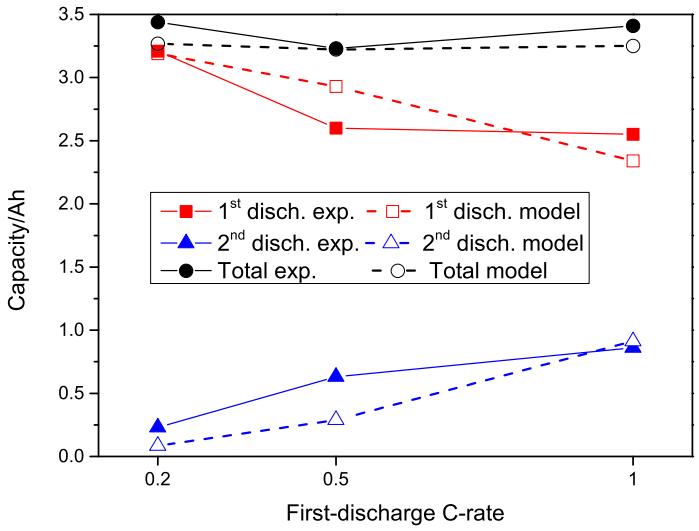

Figure 3: Experimental and modelled capacities for the first discharges at 0.2C, 0.5C, and 1C, and for the second discharges at 0.2C conducted after 5 hours of relaxation.

reduces to near-zero after 30 mins of relaxation, longer relaxation periods would not lead to further capacity recovery. The mismatch in capacity recovery rate may suggest the effective ionic diffusion coefficients in a discharged cell to be lower than the values assumed in the model. This could be caused by, for example, increased tortuosity in the discharged cathode as a result of Li_2S precipitation. Increased cathode tortuosity would lower effective ionic diffusion coefficients which further impedes ionic transport into the cathode during and after cell discharge. As mentioned previously, the empirical Bruggeman relation with an exponent of 1.5 (Eq. A22) is likely to underestimate of the change in the cathode tortuosity due to pore-clogging, as shown recently by Dysart et al [36] via stochastic micro-structure simulations.

In this modelling study, we have only pursued qualitative agreements with measured discharge curves and recoverable capacities due to several known limitations of existing Li-S models. Firstly, the present model is based on the Nernst-Plank formulation with constant ionic diffusion coefficients which is not accurate in describing the highly concentrated, multicomponent electrolyte in Li-S cells. On the other hand, the large number of ionic species in Li-S cells is likely to make the Stefan-Maxwell formulation for concentrated solution unwieldy in modelling Li-S cells, especially since the numerous concentration-dependent transport properties are difficult to obtain experimentally. Nazar et al [37] recently demonstrated the significance of cross-term diffusion coefficients in a ternary polysulfide solution containing S_4^{2-} in LiTFSI-DOL/DME. It was discovered via concentration cell and constricted diffusion measurements that S_4^{2-} could diffuse against its own concentration gradient, i.e. incongruent diffusion. Such behaviour facilitates the retention of S_4^{2-} in the cathode, which may reduce the ionic concentration gradients in the separator and alleviate mass-transport

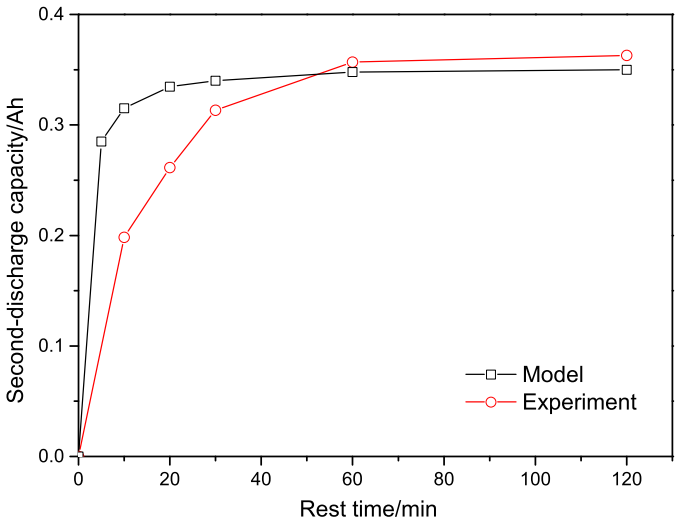

Figure 4: Experimental and modelled second-discharge capacities of a Li-S cell after different durations of relaxation. Both the first and second discharges were conducted at 1C.

limitation during cell discharge. Secondly, the model does not account for disproportionation/association reactions that are known to occur among polysulfide species. While such reactions have been under intense experimental investigations [38, 39], the exact reaction mechanisms are still not established for Li-S cells. Lastly, the present model assumes simple phenomenological expressions for the change in tortuosity and effective surface area (Eqs. A22-23) during discharge, which may not capture the precipitation-induced morphology changes very well. The morphology of the precipitates influences the effective ionic transport properties, which in turn determine the model-predicted discharge capacity and capacity recovery rate. Despite of these limitations, we have shown that it is possible to reproduce two previously not captured Li-S cell features, e.g. the reduction of low-plateau capacity at high currents and the capacity recovery effect, with simple modifications to the established Li-S model. According to the transport-limited cell behaviour modelled in this study, we suggest that in high-energy density Li-S cells where the electrolyte loading is necessarily low, the transport property of electrolyte is the limiting factor for sulfur utilisation and cell capacity.

4. Conclusions

In this study, we modelled the rate capability of a Li-S cell using a modified Kumaresan model [17] with low ionic diffusion coefficients. The slow transport of Li^+ cations towards the cathode forces active polysulfides to migrate into the separator in order to maintain charge neutrality. These trapped polysulfides lead to the experimentally observed reduction of the low-plateau capacity at high discharge rates. Furthermore, we demonstrated that the

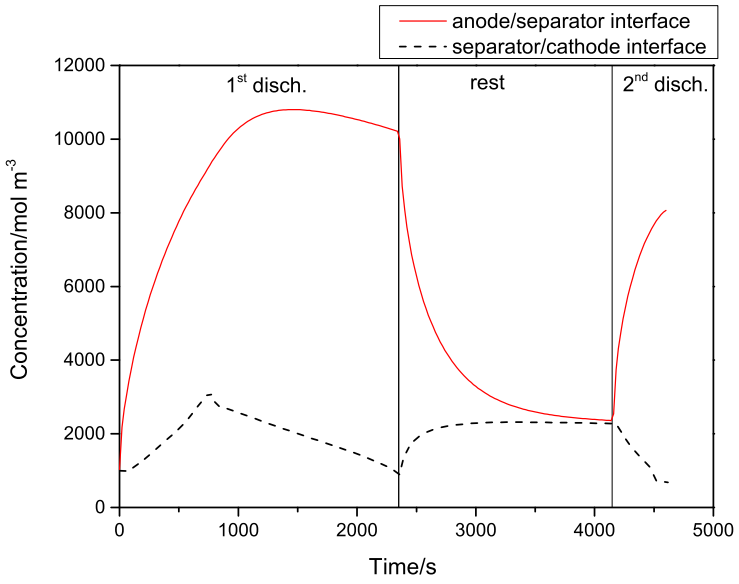

Figure 5: Simulated Li^+ ion concentrations at anode/separator interface and separator/cathode interface during a discharge-relaxation-discharge process. The discharges are simulated at 1C and the relaxation is simulated for 30 minutes.

loss in discharge capacity due to high discharge current can be recovered after just 1 hour of relaxation. This capacity recovery is due to the diffusion of trapped polysulfides back into the cathode after the cell has been disconnected. The model-predicted recoverable capacities qualitatively agree with measurements for cell discharged at different rates and relaxed for different durations.

While reducing the amount of electrolyte in Li-S cells increases their energy-density at cell-level, it also increases the electrolyte viscosity and ionic concentrations. Consequently, the transport-limitation scenario modelled in this study is likely to occur at high discharge currents thereby limiting the discharge capacity. Therefore, optimizing the electrolyte-to-sulfur mass ratio, as well as improving the ionic transport property of the electrolyte, are key in enhancing the rate capability of Li-S cells. Given the importance of the electrolyte in determining the rate capability and sulfur utilization in Li-S cells, further studies are required to determine the transport property of different Li-S electrolytes at high ionic concentrations. Determination of concentration-dependent ionic diffusion coefficients are also necessary for development of more accurate Li-S models.

Acknowledgement

The authors would like to thank the Engineering and Physical Sciences Research Council in the UK for funding this work under the Revolutionary Electric Vehicle Battery (REVB) project EP/L505298/1.

Appendix A. Model formulation

The mathematical model employed in this study is based on the 1D Li-S model developed by Kumaresan et al [17]. It considers the following Faradic reactions during discharge:

$$\frac{1}{2}S_8 + e^- \leftrightarrows \frac{1}{2}S_8^{2-}, \tag{A.1}$$

$$\frac{3}{2}S_8^{2-} + e^- \leftrightarrows 2S_6^{2-}, \tag{A.2}$$

$$S_6^{2-} + e^- \leftrightarrows \frac{3}{2}S_4^{2-}, \tag{A.3}$$

$$\frac{1}{2}S_4^{2-} + e^- \leftrightarrows S_2^{2-}, \tag{A.4}$$

$$\frac{1}{2}S_2^{2-} + e^- \leftrightarrows 2S^{2-}. \tag{A.5}$$

The dissolution and precipitation of S_8 and Li_2S are considered as the following chemical reactions:

$$S_{8(s)} \leftrightarrows S_8, \tag{A.6}$$

$$2Li^+ + S^{2-} \leftrightarrows Li_2S_{(s)}. \tag{A.7}$$

The following sections summarize the governing equations and parameters of the model.

The volume-averaged continuity equation for species i in the porous electrode (with homogeneous properties) reads

$$\frac{\partial \varepsilon C_i}{\partial t} = -\nabla \cdot \mathbf{N}_i + r_i - R_i, \tag{A.8}$$

where ε represents the pore volume fraction in the porous cathode or separator, C_i is the concentration of ionic species i (i = Li^+, S_8, S_8^{2-}, ,S_6^{2-}, S_4^{2-}, S_2^{2-}, S^{2-}, and salt anion A^-), $\mathbf{N}_i$ is the flux of species i, r_i is the electrochemical reaction rate of species i, and R_i is the precipitation/dissolution rates of species i.

Based on the dilute-solution assumption, the flux $\mathbf{N}_i$ due to diffusion and migration can be written as

$$\mathbf{N}_i = -D_i^{eff}\nabla C_i - z_i\frac{D_i^{eff}}{RT}FC_i\nabla\phi_2, \tag{A.9}$$

where F is the Faraday constant, R is the gas constant, T is temperature, D_i^{eff} is the effective diffusion coefficient of species i, z_i is the charge number of species i, and ϕ_2 is the electrolyte-phase potential. The electrochemical reaction rate r_i can be related to the current densities due to electrochemical reactions:

$$r_i = a_v \sum_j \frac{s_{i,j} i_j}{n_j F}, \tag{A.10}$$

where a_v denotes the specific area of the porous cathode, n_j denotes the number of electrons transferred in reaction j, $s_{i,j}$ is the stoichiometric coefficient of species i in electrochemical reaction j, and i_j is the current density due to the electrochemical reaction j at the solid/electrolyte interface. The rate of precipitation/dissolution reactions is given by

$$R_i = \sum_k \gamma_{i,k} R'_k, \tag{A.11}$$

where R'_k is the rate of precipitation of the solid species k ($k = \mathrm{S}_{8(s)}$, $\mathrm{Li_2S}_{(s)}$) and $\gamma_{i,k}$ is the number of moles of ionic species i in the solid species k.

The current continuity equation reads

$$\nabla \cdot \mathbf{i}_e + \nabla \cdot \mathbf{i}_s = 0, \tag{A.12}$$

where $\mathbf{i}_e$ and $\mathbf{i}_s$ are the electrolyte- and solid-phase current densities given respectively by

$$\mathbf{i}_e = F \sum_i z_i \mathbf{N}_i, \mathbf{i}_s = -\sigma \nabla \phi_1, \tag{A.13}$$

where σ is the solid-phase conductivity and ϕ_1 is the solid-phase potential. Since the current in electrolyte-phase is produced by electrochemical reactions at electrolyte/solid interfaces, the following constraint should hold:

$$\nabla \cdot \mathbf{i}_e = a_v \sum_j i_j. \tag{A.14}$$

The change in volume fraction of species k due to its precipitation/dissolution is:

$$\frac{\partial \varepsilon_k}{\partial t} = \tilde{V}_k R'_k, \tag{A.15}$$

where ε_k is the volume fraction of solid species k, and $\tilde{V}_k$ is the molar volume of k. The pore volume fraction of cathode/separator changes according to

$$\frac{\partial \varepsilon}{\partial t} = -\sum_k \tilde{V}_k R'_k. \tag{A.16}$$

The current densities due to electrochemical reactions are described by the Butler-Volmer equation

$$i_j = i_{0,j} \left\{ \prod_i \left(\frac{C_i}{C_{i,ref}} \right)^{p_{i,j}} \exp\left(\frac{0.5F}{RT} \eta_j \right) - \prod_i \left(\frac{C_i}{C_{i,ref}} \right)^{q_{i,j}} \exp\left(-\frac{0.5F}{RT} \eta_j \right) \right\}, \tag{A.17}$$

where $i_{0,j}$ is the exchange current density for reaction j, $C_{i,ref}$ is the reference (and the initial) concentration of species i, and

$$p_{i,j} = s_{i,j} \text{ for oxidized species, } q_{i,j} = -s_{i,j} \text{ for reduced species.} \tag{A.18}$$

The overpotential for reaction j is given by

$$\eta_j = \phi_1 - \phi_2 - U_{j,ref}. \tag{A.19}$$

The equilibrium potential at $C_{i,ref}$ is given by

$$U_{j,ref} = U_j^{\theta} - \frac{RT}{n_j F} \sum s_{i,j} \ln \left(\frac{C_{i,ref}}{10^3} \right), \tag{A.20}$$

where U_j^{θ} is the standard equilibrium potential at 10^3 mol m^{-3}.

The rate of precipitation/dissolution of species k takes the following form:

$$R_k^{'} = k_k \varepsilon_k \left[\prod_i (C_i)^{\gamma_{i,k}} - K_{sp,k} \right] \tag{A.21}$$

where $K_{sp,k}$ is the solubility product of k in the electrolyte, k_k is the precipitation/dissolution rate constant (Table B4). Here the effect of nucleation is represented by assuming that the precipitating amount is proportional to the amount of material already precipitated.

The effective diffusion coefficients are dependent on the porosity through the Bruggeman relation:

$$D_i^{eff} = D_i \left(\varepsilon \right)^{1.5}, \tag{A.22}$$

where D_i is the bulk diffusion coefficient of species i, and the the Bruggeman exponent is taken to be 1.5. Finally, it is assumed that the specific surface area of cathode varies with the pore volume fraction according to an empirical expression

$$a_v = a_0 \left(\frac{\varepsilon}{\varepsilon_{initial}} \right)^{1.5}, \tag{A.23}$$

where a_0 is the initial specific surface area of the cathode.

At cathode/current collector interface ($x = L_s + L_c$, where L_s and L_c are the separator and cathode thicknesses respectively), no-flux for all species applies:

$$\mathbf{N}_i(x = L_s + L_c) = 0. \tag{A.24}$$

Solid-phase current density equals to the applied current density; electrolyte-phase current density equals to zero:

$$|\mathbf{i}_s(x = L_s + L_c)| = I_{app}/A, \mathbf{i}_e(x = L_s + L_c) = 0, \tag{A.25}$$

where I_{app} is the applied current and A is the total geometric area of the current collectors.

At cathode/separator interface ($x = L_s$), continuity of species fluxes and the electrolyte-phase current density:

$$\mathbf{N}_i \left|_{L_s}^{-} \right. = \mathbf{N}_i \left|_{L_s}^{+} \right., \mathbf{i}_e \left|_{L_s}^{-} \right. = \mathbf{i}_e \left|_{L_s}^{+} \right. \tag{A.26}$$

The solid-phase current density becomes to zero:

$$\mathbf{i}_s(x = L_s) = 0. \tag{A.27}$$

At anode/separator interface ($x = 0$), the electric potential is set to zero

$$\phi_1(x = 0) = 0. \tag{A.28}$$

The species flux $\mathbf{N}_i$, other than that of Li^+, is zero:

$$\mathbf{N}_i(x = 0) = 0. \tag{A.29}$$

For Li^+, its flux is given by

$$|\mathbf{N}_{Li}(x = 0)| = \frac{i_{Li}}{F}. \tag{A.30}$$

where i_{Li} is determined from the Butler-Volmer equation Eq. A17. The electrolyte-phase current density is therefore

$$\mathbf{i}_e(x = 0) = \sum_i F\mathbf{N}_{Li}. \tag{A.31}$$

Appendix B. Model parameters and implementation

The model parameters (Table. B1 - B4) are modified from the values employed by Kumaresan et al [17] in order to fit with measured discharge curves at different C-rates. The kinetic and thermodynamic parameters for charge transfer, as well as the precipitation and dissolution parameters (Table B1 and B4) are similar to the values used in [17]. The ionic diffusion coefficients (Table B2), however, are two orders of magnitudes lower in order to represent transport-limitation condition. The geometric parameters (A, L_s, L_c) are based on the tested Li-S cell.

The 1D Li-S model was implemented and solved with Comsol Multiphysic 5.1. The 1D computational domain was discretized into 500 elements. A time-dependent solver with backward differentiation formula time stepping method and PARDISO linear systems solver was selected to solve the constant-current discharge simulations.

Table B.1: Kinetic and thermodynamic properties (adapted from [17])

Reaction (j)	$i_{0,j}$(A/m^2)	n_j	$U_j^\theta(V)$
1	0.5	1	0.0
2	1.9	1	2.41
3	0.02	1	2.35
4	0.02	1	2.23
5	2.0×10^{-4}	1	2.03
6	2.0×10^{-9}	1	2.01

Table B.2: Transport properties and initial concentrations

Species (i)	z_i	$D_{i,bulk}$ (m^2 s^{-1})	$C_{i,ref}$ (mol m^{-3})
Li^+	1	0.88×10^{-12}	1001
S_8	0	0.88×10^{-11}	19.0
S_8^{2-}	-2	3.5×10^{-12}	0.18
S_6^{2-}	-2	3.5×10^{-12}	0.32
S_4^{2-}	-2	1.75×10^{-12}	0.02
S_2^{2-}	-2	0.88×10^{-12}	5.23×10^{-7}
S^{2-}	-2	0.88×10^{-12}	8.27×10^{-10}
A^-	-1	3.5×10^{-12}	1000

Table B.3: Separator and cathode properties

Parameter	Separator	Cathode
L_s, L_c (m)	25×10^{-6}	20×10^{-6}
A (m^2)	0.28	0.28
a_0 (m^{-1})	–	132762
$\varepsilon_{initial}$	0.5	0.7
$\varepsilon_{S_{8(s)},initial}$	1×10^{-12}	0.166
$\varepsilon_{Li_2S,initial}$	1×10^{-7}	1×10^{-7}
σ (S m^{-1})	-	1

Table B.4: Precipitation and dissolution parameters (adapted from [17])

precipitate (k)	k_k	K_{sp}	$\tilde{V}_k$(m^3 mol^{-1})
$S_{8(s)}$	5.0 s^{-1}	19 mol m^{-3}	1.24×10^{-4}
Li_2S	3.45×10^{-5} m^6 mol^2 s^{-1}	1×10^2 mol^3 m	2.4×10^{-5}

References

[1] P. G. Bruce, S. A. Freunberger, L. J. Hardwick, J.-M. Tarascon, Li O 2 and Li S batteries with high energy storage, Nature Materials 11 (December) (2012) 19–30. doi:10.1038/NMAT3191.

[2] S. Urbonaite, T. Poux, P. Novk, Progress towards commercially viable lis battery cells, Advanced Energy Materials 5 (16) (2015) n/a–n/a, 1500118. doi:10.1002/aenm.201500118.
URL http://dx.doi.org/10.1002/aenm.201500118

[3] A. Rapinett, Zephyr: a high altitude long endurance unmanned air vehicle, Ph.D. thesis, University of Surrey.

[4] S. S. Zhang, Liquid electrolyte lithium/sulfur battery: Fundamental chemistry, problems, and solutions, Journal of Power Sources 231 (2013) 153–162. doi:10.1016/j.jpowsour.2012.12.102.
URL http://linkinghub.elsevier.com/retrieve/pii/S0378775312019568

[5] J. Chen, K. S. Han, W. A. Henderson, K. C. Lau, M. Vijayakumar, T. Dzwiniel, H. Pan, L. A. Curtiss, J. Xiao, K. T. Mueller, Y. Shao, J. Liu, Restricting the solubility of polysulfides in li-s batteries via electrolyte salt selection, Advanced Energy Materials (2016) n/a–n/a1600160. doi:10.1002/aenm.201600160.
URL http://dx.doi.org/10.1002/aenm.201600160

[6] Z. Li, Y. Huang, L. Yuan, Z. Hao, Y. Huang, Status and prospects in sulfur-carbon composites as cathode materials for rechargeable lithium-sulfur batteries, Carbon 92 (2015) 41–63. doi:10.1016/j.carbon.2015.03.008.
URL http://dx.doi.org/10.1016/j.carbon.2015.03.008

[7] J.-G. Wang, K. Xie, B. Wei, Advanced engineering of nanostructured carbons for lithiumsulfur batteries, Nano Energy 15 (2015) 413 – 444. doi:http://dx.doi.org/10.1016/j.nanoen.2015.05.006.
URL http://www.sciencedirect.com/science/article/pii/S2211285515002219

[8] J. Song, M. L. Gordin, T. Xu, S. Chen, Z. Yu, H. Sohn, J. Lu, Y. Ren, Y. Duan, D. Wang, Strong lithium polysulfide chemisorption on electroactive sites of nitrogen-doped carbon composites for high-performance lithium-sulfur battery cathodes, Angewandte Chemie - International Edition 54 (2015) 4325–4329. doi:10.1002/anie.201411109.

[9] G. Zhou, E. Paek, G. S. Hwang, A. Manthiram, Long-life Li/polysulphide batteries with high sulphur loading enabled by lightweight three-dimensional nitrogen/sulphur-codoped graphene sponge, Nature Communications 6 (2015) 7760. doi:10.1038/ncomms8760.
URL http://www.nature.com/doifinder/10.1038/ncomms8760

[10] J. Q. Huang, Q. Zhang, F. Wei, Multi-functional separator/interlayer system for high-stable lithium-sulfur batteries: Progress and prospects, Energy Storage Materials 1 (2015) 127–145. doi:10.1016/j.ensm.2015.09.008.
URL http://dx.doi.org/10.1016/j.ensm.2015.09.008

[11] H.-J. Peng, Q. Zhang, Designing Host Materials for Sulfur Cathodes: From Physical Confinement to Surface Chemistry, Angewandte Chemie International Edition 54 (2015) 11018–11020. doi:10.1002/anie.201505444.
URL http://doi.wiley.com/10.1002/anie.201505444

[12] M. Hagen, D. Hanselmann, K. Ahlbrecht, R. Maa, D. Gerber, J. Tbke, Lithiumsulfur cells: The gap between the state-of-the-art and the requirements for high energy battery cells, Advanced Energy Materials 5 (16) (2015) n/a–n/a, 1401986. doi:10.1002/aenm.201401986.
URL http://dx.doi.org/10.1002/aenm.201401986

[13] M. Hagen, P. Fanz, J. T??bke, Cell energy density and electrolyte/sulfur ratio in Li-S cells, Journal of Power Sources 264 (2014) 30–34. doi:10.1016/j.jpowsour.2014.04.018.
URL http://dx.doi.org/10.1016/j.jpowsour.2014.04.018

[14] J. Brückner, S. Thieme, H. T. Grossmann, S. Dörfler, H. Althues, S. Kaskel, Lithiumsulfur batteries: Influence of c-rate, amount of electrolyte and sulfur loading on cycle performance, Journal of Power Sources 268 (2014) 82 – 87. doi:http://dx.doi.org/10.1016/j.jpowsour.2014.05.143.
URL http://www.sciencedirect.com/science/article/pii/S0378775314008441

[15] S. Urbonaite, P. Novák, Importance of unimportant experimental parameters in LiS battery develop-

ment, Journal of Power Sources 249 (2014) 497–502. doi:10.1016/j.jpowsour.2013.10.095.
URL http://linkinghub.elsevier.com/retrieve/pii/S0378775313017618

[16] Y. V. Mikhaylik, J. R. Akridge, Polysulfide Shuttle Study in the Li/S Battery System, Journal of The Electrochemical Society 151 (11) (2004) A1969. doi:10.1149/1.1806394.
URL http://jes.ecsdl.org/cgi/doi/10.1149/1.1806394

[17] K. Kumaresan, Y. Mikhaylik, R. E. White, A Mathematical Model for a LithiumSulfur Cell, Journal of The Electrochemical Society 155 (8) (2008) A576. doi:10.1149/1.2937304.
URL http://jes.ecsdl.org/cgi/doi/10.1149/1.2937304

[18] D. N. Fronczek, W. G. Bessler, Insight into lithiumsulfur batteries: Elementary kinetic modeling and impedance simulation, Journal of Power Sources 183 (2013) 183–188. doi:10.1016/j.jpowsour.2013.02.018.
URL http://linkinghub.elsevier.com/retrieve/pii/S0378775313002814

[19] A. F. Hofmann, D. N. Fronczek, W. G. Bessler, Mechanistic modeling of polysulfide shuttle and capacity loss in lithium-sulfur batteries, Journal of Power Sources 259 (2014) 300–310. doi:10.1016/j.jpowsour.2014.02.082.
URL http://linkinghub.elsevier.com/retrieve/pii/S0378775314002754

[20] M. Ghaznavi, P. Chen, Sensitivity analysis of a mathematical model of lithiumsulfur cells part I: Applied discharge current and cathode conductivity, Journal of Power Sources 257 (2014) 394–401. doi:10.1016/j.jpowsour.2013.10.135.
URL http://linkinghub.elsevier.com/retrieve/pii/S0378775313018028

[21] M. Ghaznavi, P. Chen, Sensitivity analysis of a mathematical model of lithiumsulfur cells: Part II: Precipitation reaction kinetics and sulfur content, Journal of Power Sources 257 (2014) 402–411. doi:10.1016/j.jpowsour.2013.12.145.
URL http://linkinghub.elsevier.com/retrieve/pii/S0378775314001219

[22] M. Ghaznavi, P. Chen, Analysis of a Mathematical Model of Lithium-Sulfur Cells Part III: Electrochemical Reaction Kinetics, Transport Properties and Charging, Electrochimica Acta 137 (2014) 575–585. doi:10.1016/j.electacta.2014.06.033.
URL http://dx.doi.org/10.1016/j.electacta.2014.06.033

[23] T. Zhang, M. Marinescu, L. O'Neill, M. Wild, G. Offer, Modeling the voltage loss mechanisms in lithium-sulfur cells: the importance of electrolyte resistance and precipitation kinetics, Phys. Chem. Chem. Phys. 17 (2015) 22581–22586. doi:10.1039/C5CP03566J.
URL http://dx.doi.org/10.1039/C5CP03566J

[24] M. Marinescu, T. Zhang, G. J. Offer, A zero dimensional model of lithium-sulfur batteries during charge and discharge, Phys. Chem. Chem. Phys. 18 (2016) 584–593. doi:10.1039/C5CP05755H.
URL http://dx.doi.org/10.1039/C5CP05755H

[25] S. M. Al-Mahmoud, J. W. Dibden, J. R. Owen, G. Denuault, N. Garcia-Araez, A simple, experiment-based model of the initial self-discharge of lithium-sulphur batteries, Journal of Power Sources 306 (2016) 323–328. doi:10.1016/j.jpowsour.2015.12.031.
URL http://linkinghub.elsevier.com/retrieve/pii/S0378775315306443

[26] T. Danner, G. Zhu, A. F. Hofmann, A. Latz, Modeling of nano-structured cathodes for improved lithium-sulfur batteries, Electrochimica Acta 184 (2015) 124–133. doi:10.1016/j.electacta.2015.09.143.
URL http://dx.doi.org/10.1016/j.electacta.2015.09.143

[27] F. Y. Fan, W. C. Carter, Y.-M. Chiang, Mechanism and Kinetics of Li2S Precipitation in LithiumSulfur Batteries, Advanced Materials 27 (2015) 5203–5209. doi:10.1002/adma.201501559.
URL http://onlinelibrary.wiley.com/doi/10.1002/adma.201501559/abstract

[28] C. E. Parfitt, Characterization, modelling and management of lithium-sulphur batteries for spacecraft applications, Ph.D. thesis, University of Warwick.

[29] S. Walu, C. Barchasz, R. Bouchet, J.-C. Leprtre, J.-F. Colin, J.-F. Martin, E. Elkam, C. Baehtz, F. Alloin, Lithium/sulfur batteries upon cycling: Structural modifications and species quantification by in situ and operando x-ray diffraction spectroscopy, Advanced Energy Materials 5 (16) (2015) n/a–n/a, 1500165. doi:10.1002/aenm.201500165.

URL http://dx.doi.org/10.1002/aenm.201500165

[30] Y.-C. Lu, Q. He, H. A. Gasteiger, Probing the lithiumsulfur redox reactions: A rotating-ring disk electrode study, The Journal of Physical Chemistry C 118 (11) (2014) 5733–5741. arXiv:http://dx.doi.org/10.1021/jp500382s, doi:10.1021/jp500382s.
URL http://dx.doi.org/10.1021/jp500382s

[31] U. Tilstam, Sulfolane: A versatile dipolar aprotic solvent, Organic Process Research & Development 16 (7) (2012) 1273–1278. arXiv:http://dx.doi.org/10.1021/op300108w, doi:10.1021/op300108w.
URL http://dx.doi.org/10.1021/op300108w

[32] B. Tjaden, S. J. Cooper, D. J. Brett, D. Kramer, P. R. Shearing, On the origin and application of the bruggeman correlation for analysing transport phenomena in electrochemical systems, Current Opinion in Chemical Engineering 12 (2016) 44 – 51, nanotechnology Separation Engineering. doi:http://dx.doi.org/10.1016/j.coche.2016.02.006.
URL http://www.sciencedirect.com/science/article/pii/S2211339816300119

[33] S. Cooper, D. Eastwood, J. Gelb, G. Damblanc, D. Brett, R. Bradley, P. Withers, P. Lee, A. Marquis, N. Brandon, P. Shearing, Image based modelling of microstructural heterogeneity in lifepo4 electrodes for li-ion batteries, Journal of Power Sources 247 (2014) 1033 – 1039. doi:http://dx.doi.org/10.1016/j.jpowsour.2013.04.156.
URL http://www.sciencedirect.com/science/article/pii/S0378775313007763

[34] V. Kolosnitsyn, E. Kuzmina, E. Karaseva, S. Mochalov, A study of the electrochemical processes in lithiumsulphur cells by impedance spectroscopy, Journal of Power Sources 196 (3) (2011) 1478–1482. doi:10.1016/j.jpowsour.2010.08.105.
URL http://linkinghub.elsevier.com/retrieve/pii/S0378775310015909

[35] N. A. Cañas, K. Hirose, B. Pascucci, N. Wagner, K. A. Friedrich, R. Hiesgen, Investigations of lithium-sulfur batteries using electrochemical impedance spectroscopy, Electrochimica Acta 97 (2013) 42–51. doi:10.1016/j.electacta.2013.02.101.
URL http://linkinghub.elsevier.com/retrieve/pii/S0013468613003460

[36] A. D. Dysart, J. C. Burgos, A. Mistry, C.-F. Chen, Z. Liu, C. N. Hong, P. B. Balbuena, P. P. Mukherjee, V. G. Pol, Towards next generation lithium-sulfur batteries: Non-conventional carbon compartments/sulfur electrodes and multi-scale analysis, Journal of The Electrochemical Society 163 (5) (2016) A730–A741. arXiv:http://jes.ecsdl.org/content/163/5/A730.full.pdf+html, doi:10.1149/2.0481605jes.
URL http://jes.ecsdl.org/content/163/5/A730.abstract

[37] M. Safari, C. Y. Kwok, L. F. Nazar, Transport properties of polysulfide species in lithiumsulfur battery electrolytes: Coupling of experiment and theory, ACS Central Science 0 (0) (0) null. arXiv:http://dx.doi.org/10.1021/acscentsci.6b00169, doi:10.1021/acscentsci.6b00169.
URL http://dx.doi.org/10.1021/acscentsci.6b00169

[38] R. Xu, J. Lu, K. Amine, Progress in mechanistic understanding and characterization techniques of li-s batteries, Advanced Energy Materials 5 (16) (2015) n/a–n/a, 1500408. doi:10.1002/aenm.201500408.
URL http://dx.doi.org/10.1002/aenm.201500408

[39] M. Wild, L. O'Neill, T. Zhang, R. Purkayastha, G. Minton, M. Marinescu, G. J. Offer, Lithium sulfur batteries, a mechanistic review, Energy Environ. Sci. 8 (2015) 3477–3494. doi:10.1039/C5EE01388G.
URL http://dx.doi.org/10.1039/C5EE01388G